

The interaction of intense femtosecond laser pulses with argon microdroplets studied near the soft x-ray emission threshold

R. Irsig¹, M. Shihab^{1,2}, L. Kazak¹, T. Bornath¹,
J. Tiggesbäumker^{1,*}, R. Redmer¹, and K.-H. Meiwes-Broer¹

¹ Institut für Physik, Universität Rostock, 18059 Rostock, Germany

² Department of Physics, Faculty of Science, Tanta University, Tanta 31527, Egypt

* E-mail : josef.tiggesbaeumker@uni-rostock.de

Abstract. The extreme ultraviolet plasma emission from liquid micro-sized argon droplets exposed to intense near-infrared laser pulses has been investigated. Emission from the warm dense matter targets is recorded in a spectral range in between 16 and 30 nm at laser intensities of 10^{14} W/cm². Above the emission threshold, soft x-ray radiation exponentially increases with the pulse energy whereby a strong dependence of the yields on the pulse duration is observed, which points at an effective electron collisional heating of the microplasma by inverse bremsstrahlung. Accompanying hydrodynamic simulations reveal the temporal and spatial development of the microplasma conditions. The good agreement in between the measured and calculated emission spectra as well as the extracted electron temperatures confirm that hydrodynamic simulations can be applied in the analysis of strongly excited droplets.

1. Introduction

The interaction of intense near-infrared (NIR) laser light with small particles has been of particular interest in the last decades, since it allows to study matter of finite size under extreme conditions [1--7]. Due to the strong absorption capabilities, nanoparticles are effectively transformed into nanoplasmas [8], which results in the emission of highly charged and energetic ions [9--11] and fast electrons [12, 13]. The generation of short wavelength radiation [14, 15] and high harmonics [16, 17] allows to resolve further details of the size-limited plasma conditions [4, 18--21].

With microdroplets, the dimension of the target becomes comparable to NIR laser wavelength and propagation phenomena show up. The laser light wave penetrates into the droplet up to a region where the critical density in the plasma is achieved. In addition, the spatial density scale length is much lower compared to, e.g., the Ti:sapphire laser wavelength of 800 nm. Hence, absorption of radiation occurs only near the surface of the droplet. The resulting hot plasma is far from equilibrium. As a consequence, the dynamics of the laser-produced plasma layer has to be simulated in order to resolve details of the processes involved. The microplasma may retroact on the light propagation, further influencing the absorption properties including extreme ultraviolet (EUV) re-absorption. As a result of strong electron density gradients, wave propagation phenomena show up, e.g., shock waves [22], wave breaking and turbulence [23]. The limited size of the target space charge confinement of hot electrons will lead to an efficient coupling of the laser radiation into the particle [24]. Particle-in-cell simulations show that an inhomogeneous plasma layer develops which extends deeper into the droplets than expected from classical predictions [25].

Beside particle plasma diagnostics, radiation has proven to give meaningful information to characterize the complex dynamics in microplasmas [26,27]. For example, intense short-wavelength radiation from extended-ultraviolet free-electron lasers can isochorically heat particles, whereby self-Thomson scattering can be exploited to characterize the resulting warm dense matter (WDM) state [28]. EUV-pump--EUV-probe studies were successful in mapping the solid-to-plasma transition in real time [29]. Combining time-resolved soft x-ray diagnostics with microplasma generation by intense NIR laser pulses remains a challenge due to the initially incomplete spatial heating. WDM targets also represent laboratory systems to simulate conditions found in planets and are thus relevant for astrophysical research [30]. Finally, the short wavelength emission from particles in a molecular beam have potential for applications like high repetition rate table-top x-ray sources [31], because the technique provides a regenerative target and nearly debris-free conditions.

In this contribution we address in a joint experimental and theoretical project the generation of the transient plasma state by analyzing the resulting EUV radiation from an NIR laser-induced argon microplasma. In a simplified view of the interaction, ionization of the liquid microdroplets is triggered by tunnel ionization. As the electron quiver amplitude at 10^{14} W/cm² [32] exceeds the interatomic distances in the liquid [33], efficient collisional ionization into high charge states will take place producing a plasma at near solid-state density. The thin plasma sheet provides in the following for an efficient heating by inverse bremsstrahlung leading to a strong nonlinear dynamics. After the impact of the laser pulse, the outward expansion of the plasma

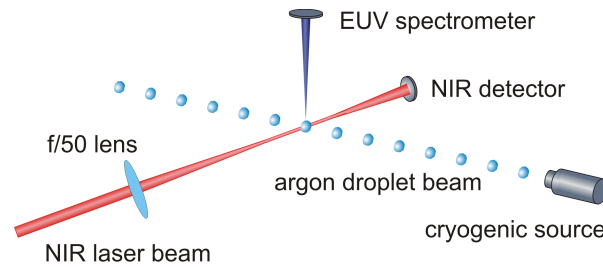


Figure 1. (color online) Schematic view of the experimental setup. NIR femtosecond laser pulses at intensities of 10^{14} W/cm² are focused onto a beam of argon microdroplets generated by a cryogenic source. In the strong-field interaction, a warm dense matter target is produced. Highly charged ions present in the microplasma emit characteristic short wavelength radiation. The EUV spectra are recorded between 16 and 30 nm (41 to 77 eV) by a home-built flat-field spectrometer aligned perpendicular to the laser-droplet plane.

layer leads to a decrease in the plasma density and an adiabatic cooling [34]. Soft x-ray emission as a characteristic fluorescence signature of the plasma conditions occurs on a pico- to nanosecond time scale.

In contrast to other experiments on droplets at near relativistic intensities, e.g. [5, 20], moderate laser intensities are applied in order to study the dynamics close to the argon tunnel ionization threshold of $2 \cdot 10^{14}$ W/cm² [35]. To solidify the investigation the experiments are accompanied by theoretical work, i.e. the experimental average electron temperatures extracted from the EUV spectra will be compared to simulations. The good agreement of the theoretical results to the experiments point out that the microplasma dynamics can be described well by 1D hydrodynamical codes.

2. Experiment

To effectively conduct the experiment, a regenerative high-density target is utilized, i.e., a liquid jet source similar to the one used in [36]. In short, the microdroplet beam is generated by expanding liquefied argon gas (100 K at 5 bar) through a 5 μ m nozzle into vacuum forming a continuous filament. Due to surface vibrations, the filament undergoes a Rayleigh breakup and splits into monodisperse droplets [37] with diameters of approximately 9 μ m. The droplets are irradiated by pulses from a Ti:sapphire laser system with a center wavelength at 810 nm and a pulse repetition rate of 1 kHz. The laser beam is focused with a f/50 lens, see Fig. 1. Experiments are performed with pulse durations between 100 fs and 800 fs and pulse energies up to 1.5 mJ, which corresponds to a maximal pulse intensity of $9 \cdot 10^{14}$ W/cm² in the interaction region. The EUV emission produced in the strong-field interaction with the

droplets is recorded by a home-built EUV spectrometer aligned 90° to both laser and droplet beam. The spectrometer consists of an aberration corrected flat-field grating as single optical element [38]. A back-illuminated CCD camera (Andor, model *Newton 940 DO*) serves for EUV photon detection. A 200 nm aluminum foil is used to suppress scattered laser light. With the instrument, spectra in a range between 16 and 30 nm can be recorded.

As the Rayleigh breakup takes place spontaneously, a temporal synchronization between droplets and laser pulses cannot be achieved. In order to estimate the efficiency at which droplets are hit by laser radiation, the transmitted energy of single pulses after passing the interaction region is determined (NIR detector in Fig. 1). From the analysis we found that about 70% of the pulses interact with a droplet. To suppress signal fluctuations spectra are integrated over 10^4 laser pulses.

3. Simulation

The interaction of intense femtosecond laser pulses with microdroplets is studied using the radiation-hydrodynamic HELIOS code [39]. Briefly, HELIOS provides a Lagrangian reference frame where electrons and ions are assumed to be co-moving. Pressure contributions to the equation of motion stem from electrons, ions and radiation. Separate ion and electron temperatures and flux-limited Spitzer thermal conductivity are assumed. Deviations from local thermodynamic equilibrium conditions are accounted for by solving multi-level atomic rate equations at each time step in the simulation. The laser energy is deposited via inverse bremsstrahlung as well as bound-bound and bound-free transitions using an SESAME-like equation of state. The EUV emission of the microdroplets is calculated using SPECT3D based on the temperature and density of the plasma plume expected via radiation-hydrodynamic simulations. SPECT3D is a collisional-radiative code [40] whereas the radiation incident at a detector is estimated by solving the radiative transfer equation along a series of lines-of-sight through the plasma grid. Atomic cross section data are generated using a collection of publicly available codes [41--45], where different processes are considered, such as excitation, electron-impact ionization, photoionization, radiative recombination, autoionization, and dielectronic recombination. In addition, continuum lowering effects are implemented using an occupation probability model.

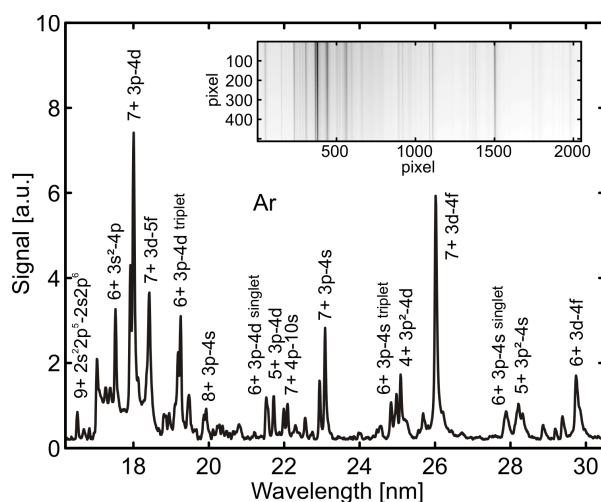


Figure 2. EUV spectrum measured after exposure of argon microdroplets by intense ultrashort laser pulses at intensities of $8 \cdot 10^{14}$ W/cm². Several emission lines resulting from argon charge states Ar⁴⁺ to Ar⁹⁺ can clearly be resolved. Inset: Raw data of the flat-field spectrometer.

4. Experimental results

Fig. 2 shows an EUV spectrum recorded after exposure of microdroplets to 100 fs laser pulses at intensities of $8 \cdot 10^{14}$ W/cm². The characteristic line pattern can be assigned to atomic transitions from Ar⁴⁺ to Ar⁹⁺ [19, 46]. Note that under the given intensity conditions, the laser field ionization of single atoms only leads to charge states up to Ar³⁺ [35] indicating that anticipated processes like collisional ionization must contribute. In the following we concentrate on the ion species Ar⁷⁺ as it represents a characteristic and dominant fingerprint of the microplasma. Fig. 3 shows the normalized yields of the Ar⁷⁺ 3p-4d transition line depending on the pulse energy for pulse durations of 100 fs and 700 fs. A strong increase of the EUV signal is observed beyond a threshold of 1.1 mJ. At 700 fs and 1.1 mJ, the laser intensity matches the argon tunnel ionization threshold [35], but is a factor of 7 higher for 100 fs pulses. One obtains no significant change in the emission threshold behavior if shorter pulses are used. Charging of the droplet by only tunnel ionization is thus not sufficient to cause plasma EUV emission. The strong nonlinear dependence around the EUV threshold points to an avalanche-like process whereby collisional ionization and inverse bremsstrahlung efficiently heat the target. For both pulse durations, the yields enhance by more than two orders of magnitude, although the pulse energy only increases from 1.1 to 1.5 mJ.

Whereas the plot in Fig. 3 appears to suggest that the pulse duration is of little importance, a closer look reveals a differentiated perspective. Fig. 4 shows the dependence of the Ar⁷⁺

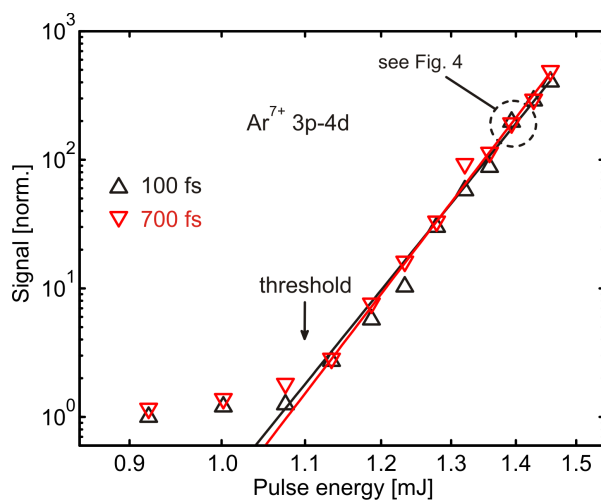


Figure 3. (color online) Experimental Ar^{7+} 3p-4d yields on a double logarithmic scale as function of the laser pulse energy for selected pulse durations. The data are normalized to the value obtained with 0.92 mJ and 100 fs. The pronounced nonlinear increase above laser energies of about 1.1 mJ points at the highly nonlinear plasma dynamics. Similar findings have been obtained for all other transitions present in the spectrum in Fig 2.

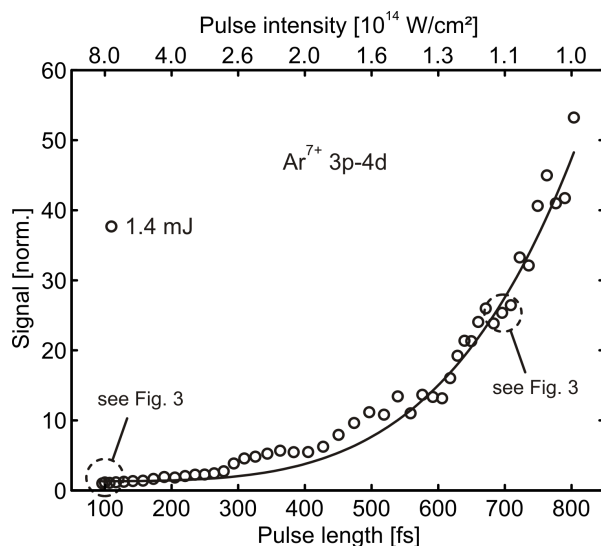


Figure 4. Experimental dependence of the Ar^{7+} 3p-4d EUV signal on pulse duration for a given pulse energy of 1.4 mJ (see Fig. 3). The data are normalized to the pulse duration of 100 fs. The yields increase with pulse length although the pulse intensity decreases (upper scale).

3p-4d emission on the pulse duration for a given pulse energy of 1.4 mJ. Apparently, an extended heating period with stretched pulses at energies above the emission threshold is more effective even though the laser intensity decreases. We emphasize that similar findings have been obtained in experiments on small clusters [47].

From the emission spectra obtained in the experiment, relevant plasma parameters as for

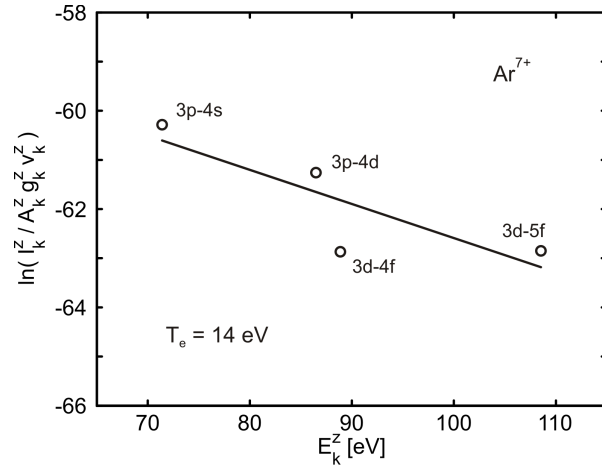


Figure 5. Extraction of the electron temperature from a Boltzmann plot using the emission lines of Ar^{7+} . The corresponding spectrum has been recorded with a laser pulse energy of 1.4 mJ and a pulse duration of 100 fs. From the experimental data $T_e=14$ eV is deduced. Note that the transition Ar^{7+} 4p-10s from Fig. 2 is not included, as the Einstein coefficient is not available in this case. As well, determination from other emission lines, e.g. Ar^{6+} , could give a slightly shifted T_e . The Boltzmann plot method is sensitive only to the spatial area, where a certain ion species is abundant and contributes to the signal significantly.

example the electron temperature T_e can be extracted. We apply the Boltzmann plot method to determine T_e from line intensities [48] assuming the microplasma to be at local thermodynamic equilibrium (LTE) at the time of the EUV emission. Briefly, the density n_k of a certain ion species k as function of T_e can be described by a Boltzmann distribution $n_k = n_0 g_k / Z_k(T_e) \exp(-E_k / k_B T_e)$, where n_0 is the total density, g_k the statistical weight, $Z_k(T_e)$ the partition function, E_k the upper energy level and k_B the Boltzmann constant. The relative line intensity I_k^z of a certain transition z in the charge state k scales by $I_k^z \sim h \nu_k^z A_k^z n_k^z$, with ν_k^z and A_k^z the frequency and Einstein coefficients, respectively. One can derive a linear equation in the form of $\ln(I_k^z / A_k^z g_k^z \nu_k^z) = -E_k^z / k_B T_e + \text{const}$. A linear regression taking into account the emission lines of a given charge state allows to extract T_e . Fig. 5 shows the Boltzmann plot analysis for Ar^{7+} giving a value of T_e of about 14 eV ($1 \pm 20\%$) in this case. The accuracy in the determination of T_e is comparable to other work in the warm dense matter regime, e.g. [28].

5. Computational results

In the HELIOS calculations, argon droplets are considered with an initial diameter of 10 μm and a mass density of $\rho_0 = 1.4 \text{ g/cm}^3$ irradiated by intense laser pulses at 800 nm center

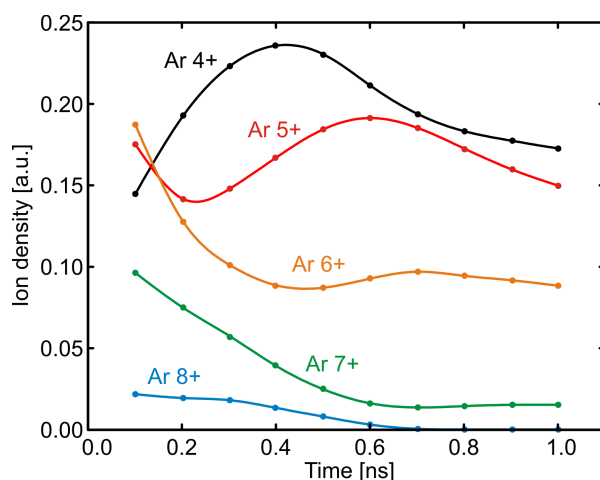


Figure 6. (color online) Calculated temporal density distribution of argon ion species generated in the plasma layer for laser pulses with 100 fs and 2.1 mJ. (Time steps of 100 ps are used. The curves are drawn to guide eyes.) Charge states from Ar^{4+} to Ar^{8+} are shown. Ar^{9+} is not observed in the simulation. Note that in the interaction with the laser pulse itself, up to Ar^{3+} can significantly be produced by tunnel ionization. The arise of higher charge states indicates the contribution of inverse bremsstrahlung and collision ionization to the plasma heating. The plasma dynamics lasts over nanoseconds after the laser pulse trigger at $t = 0$.

wavelength. Fig. 6 shows the temporal ion density distributions ρ_q of various charge states for laser pulses with 100 fs pulse length and 2.1 mJ pulse energy. The charge state abundances are captured up to nanoseconds after the laser pulse exposure at $t = 0$. The ionization kinetics are caused by collisional excitation and recombination as well as collective processes in the plasma layer. In the expansion, electron-ion recombination leads to a general decrease of ρ_q . The short-term enhancement in the ion densities of certain charge states after some hundred picoseconds can be traced back to electron localization reducing the value of q in higher charged Ar^{q+} .

Fig. 7 displays the spatial evolution of the mass density and electron temperature as well as the ionization fraction of Ar^{7+} at $t = 100$ ps. Most of the inner part of the droplet (left to dashed line) has a low temperature as the laser radiation is shielded by the plasma layer. As a consequence, the mass density inside the droplet remains at its initial value ρ_0 . A plasma compression is observed in the surface region. A hot, highly ionized plasma layer extends over tens of micrometers outwards. The mass density drops - depending on the laser pulse energy - to values as low as 10^{-4} g/cm³ beyond 40 μm . The composition of the plasma varies with distance. An enhanced abundance of Ar^{7+} (Fig. 7 bottom) is observed in a layer between 20 and 40 μm approaching values of 10 to 40 % of the total density in the plasma plume. In general, only a minor dependence of T_e and ρ on the pulse energy is obtained

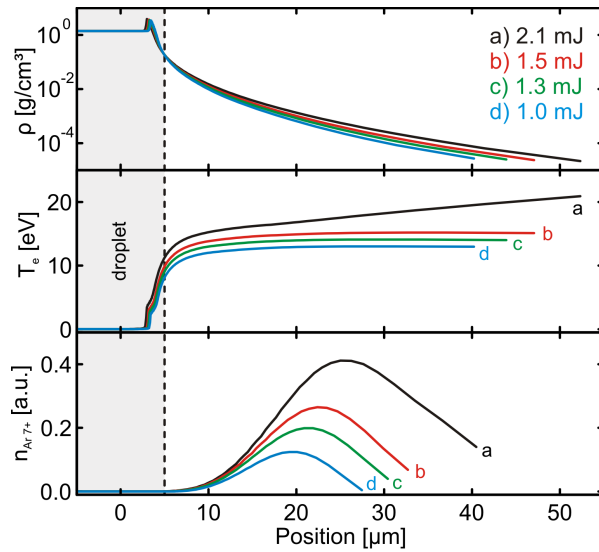


Figure 7. (color online) Snapshots of spatial distributions of mass density ρ (top), electron temperature T_e (center) and Ar^{7+} ionization fraction $n_{\text{Ar}^{7+}}$ (bottom) calculated for $t = 100$ ps after the laser pulse trigger. Different pulse energies at a constant pulse length of 100 fs are used. The initially irradiated surface of the microdroplet is located at a position of $5 \mu\text{m}$, the plasma expands to the right.

for the considered range of parameters. The inner region of the microdroplet is still almost unaffected. However, in particular hot electrons penetrate and slowly heat-up the droplet core leading to an increasing ionization. After $t = 1$ ns, the droplet is almost fully ionized as illustrated in Fig. 8. Interestingly and in accordance with the experimental findings, see Fig. 4, longer pulses extend the heating period and lead to an increase in the temperature of the microplasma and, thereby, enhanced population of higher ionization states. Whereas the inner region of the droplets is nearly unaffected by a variation of the pulse duration, the temperature near the surface and, especially, in the outer plasma region increases applying longer pulses.

Finally we like to compare the experimental findings with the results obtained in the simulations. For this purpose the resulting soft x-ray spectra using the SPECT3D software package are computed [40]. For given T_e the relative line intensities are calculated and compared to the measurement, see Fig. 9. For a complete description, one should consider that the EUV plasma emission will originate from the full period of the microplasma expansion. Hence, only averaged values of, e.g., T_e can be extracted from the measurements. Taking this into account, a good agreement is found between experiment and theory as details of the spectra match almost consistently, see Fig. 10. The corresponding plasma electron temperatures also agree although the calculations have been performed using a one-dimensional hydrodynamic

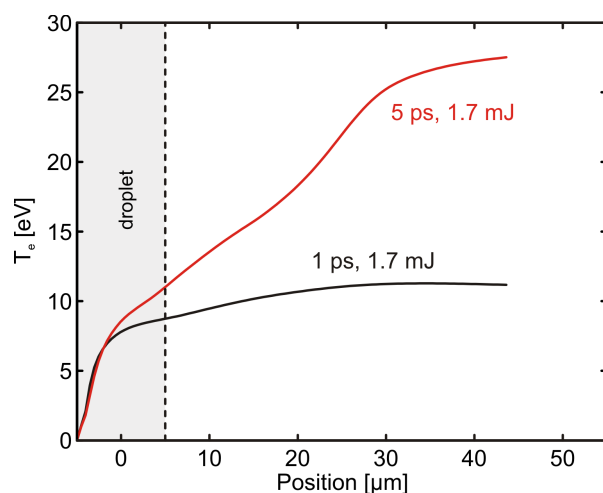


Figure 8. (color online) Snapshots of calculated spatial distributions of the electron temperature T_e at $t = 1$ ns for different pulse durations indicating that the interior of the droplet will be almost fully ionized. The influence of the pulse duration is greatest for the outer surface plasma layer.

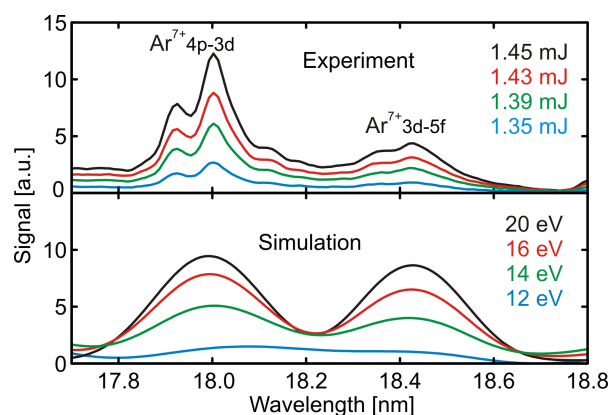


Figure 9. (color online) Dependence of the signal of selected nearby emission lines (Ar^{7+} 4p-3d and 3d-5f) on the plasma conditions. Experimental results for different laser energies (top) are compared with SPECT3D calculations for different electron temperatures (bottom). The experimentally observed enhanced line intensities with increased laser pulse energies can be traced back theoretically to an increase of temperature in the plasma layer.

code which cannot reveal the full spatial evolution of the plasma.

6. Conclusion

Soft x-ray radiation from argon microdroplets irradiated by intense femtosecond pulses has been analyzed near the EUV emission threshold in a joint experimental and theoretical study. At given pulse energy, charging of the droplets can be controlled by the pulse duration. The longer impact time supports plasma heating leading to an enhancement of the EUV

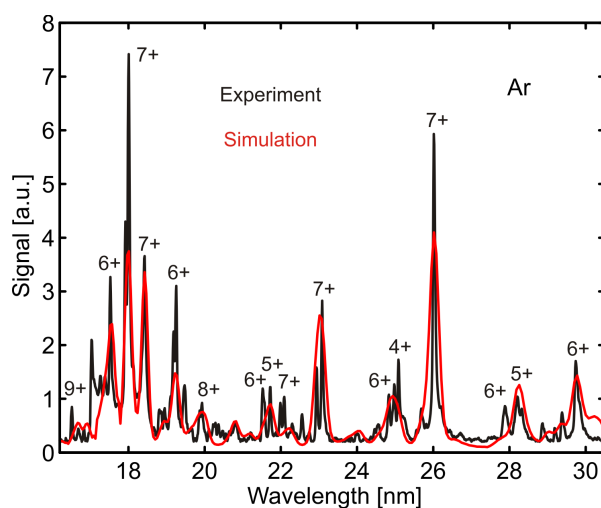


Figure 10. (color online) Experimentally recorded EUV emission taken at 1.4 mJ pulse energy (black) and calculated spectrum for an electron temperature of 16 eV (red), respectively. Equal charge states and atomic transitions are observed and thus similar plasma conditions can be assumed.

emission. Hydrodynamic simulations reveal that plasma formation initially takes place on the surface of the droplet. In the expansion of the plasma layer spatial and temporal charge state distributions change up to nanoseconds. Whereas the outer plasma cools down in the adiabatic expansion, the inner region of the droplet heats up on a comparable time scale. The experimental spectrum contains contributions from the full development of the microplasma expansion. Nevertheless average electron temperatures extracted from the EUV emission signal are found to be in good agreement with hydrodynamical (HELIOS) and collisional-radiative (SPECT3D) simulations. In further work the analysis of the plasma parameters may be improved by applying the Saha-Boltzmann distribution instead of the Boltzmann distribution.

7. Acknowledgment

We gratefully acknowledge financial support by the DFG within the SFB 652 and by the BMBF within the FSP 302.

- [1] Krainov V P and Smirnov M B 2002 *Phys. Rep.* **370** 237--331
- [2] Saalman U, Siedschlag C and Rost J M 2006 *J. Phys. B* **39** R39
- [3] Fennel T, Meiwes-Broer K H, Tiggesbäumker J, Reinhard P G, Dinh P M and Suraud E 2010 *Rev. Mod. Phys.* **82** 1793
- [4] McNaught S J, Fan J, Parra E and Milchberg H M 2001 *Appl. Phys. Lett.* **79** 4100--4102
- [5] Wieland M, Wilhein T, Faubel M, Ellert C, Schmidt M and Sublemontier O 2001 *Appl. Phys. B* **72** 591--597
- [6] Parra E, McNaught S J, Fan J and Milchberg H M 2003 *Appl. Phys. A* **77** 317--323
- [7] Garnov S V, Bukin V V, Malyutin A A and Strelkov V V 2009 Ultrafast space-time and spectrum-time resolved diagnostics of multicharged femtosecond laser microplasma *AIP Conf. Proc.* vol 1153 (AIP) pp 37--48
- [8] Ditmire T, Smith R A, Tisch J W G and Hutchinson M H R 1997 *Phys. Rev. Lett.* **78** 3121
- [9] Snyder E M, Buzza S A and Castleman Jr A W 1996 *Phys. Rev. Lett.* **77** 3347
- [10] Lezius M, Dobosz S, Normand D and Schmidt M 1998 *Phys. Rev. Lett.* **80** 261--264
- [11] Köller L, Schumacher M, Köhn J, Teuber S, Tiggesbäumker J and Meiwes-Broer K H 1999 *Phys. Rev. Lett.* **82** 3783--3786
- [12] Springate E, Aseyev S A, Zamith S and Vrakking M J J 2003 *Phys. Rev. A* **68** 053201
- [13] Passig J, Irsig R, Truong N X, Fennel T, Tiggesbäumker J and Meiwes-Broer K H 2012 *New J. Phys.* **14** 085020
- [14] McPherson A, Thompson B D, Borlsov A B, Boyer K and Rhodes C K 1994 *Nature* **370** 631--634
- [15] Issac R C, Vieux G, Ersfeld B, Brunetti E, Jamison S P, Gallacher J, Clark D and Jaroszynski D A 2004 *Phys. Plas.* **11** 3491--3496
- [16] Tisch J W G, Ditmire T, Fraser D J, Hay N, Mason M B, Springate E, Marangos J P and Hutchinson M H R 1997 *J. Phys. B* **30** L709
- [17] Bulanov S V, Naumova N M and Pegoraro F 1994 *Phys. Plas.* **1** 745--757
- [18] Ditmire T, Donnelly T, Rubenchik A M, Falcone R W and Perry M D 1996 *Phys. Rev. A* **53** 3379--3402
- [19] Zweiback J, Ditmire T and Perry M D 1999 *Phys. Rev. A* **59** R3166--R3169
- [20] Parra E, Alexeev I, Fan J, Kim K Y, McNaught S J and Milchberg H M 2000 *Phys. Rev. E* **62** R5931--R5934
- [21] Prigent C, Deiss C, Lamour E, Rozet J P, Vernhet D and Burgdörfer J 2008 *Phys. Rev. A* **78** 053201
- [22] Zeld'ovich Y B and Raizer Y P 1966 *Physics of shock waves and high-temperature hydrodynamic phenomena* (Academic Press)
- [23] Varin C, Peltz C, Brabec T and Fennel T 2012 *Phys. Rev. Lett.* **108** 175007
- [24] Sperling P, Liseykina T, Bauer D and Redmer R 2013 *New J. Phys.* **15** 025041
- [25] Liseykina T V and Bauer D 2013 *Phys. Rev. Lett.* **110** 145003
- [26] Glenzer S H and Redmer R 2009 *Rev. Mod. Phys.* **81** 1625--1663
- [27] Ostrikov K, Neyts E C and Meyyappan M 2013 *Adv. Phys.* **62** 113--224
- [28] Fäustlin R R, Bornath T, Döppner T, Düsterer S, Förster E, Fortmann C, Glenzer S H, Göde S, Gregori G, Irsig R, Laarmann T, Lee H J, Li B, Meiwes-Broer K H, Mithen J, Nagler B, Przystawik A, Redlin H, Redmer R, Reinholz H, Röpke G, Tavella F, Thiele R, Tiggesbäumker J, Toleikis S, Uschmann I, Vinko S M, Whitcher T, Zastra U, Ziaja B and Tschentscher T 2010 *Phys. Rev. Lett.* **104** 125002
- [29] Zastra U, Sperling P, Harmand M, Becker A, Bornath T, Bredow R, Dziarzhytski S, Fennel T, Fletcher L B, Förster E, Göde S, Gregori G, Hilbert V, Hochhaus D, Holst B, Laarmann T, Lee H J, Ma T, Mithen J P, Mitzner R, Murphy C D, Nakatsutsumi M, Neumayer P, Przystawik A, Roling S, Schulz M, Siemer B, Skruszewicz S, Tiggesbäumker J, Toleikis S, Tschentscher T, White T, Wöstmann M, Zacharias H, Döppner T, Glenzer S H and Redmer R 2014 *Phys. Rev. Lett.* **112** 105002
- [30] Guillot T 1999 *Science* **286** 72--77
- [31] Stiel H, Vogt U, Ter-Avetisyan S, Schnurer M, Will I and Nickles P V 2002 *Proc. SPIE* **4781** 26--34
- [32] Krainov V P, Smirnov B M and Smirnov M B 2007 *Physics-Uspekhi* **50** 907
- [33] Henshaw D G, Hurst D G and Pope N K 1953 *Phys. Rev.* **92** 1229
- [34] Shihab M, Abou-Koura G H and El-Siragy N M 2016 *Appl. Phys. B* **122** 146

- [35] Augst S, Strickland D, Meyerhofer D D, Chin S L and Eberly J H 1989 *Phys. Rev. Lett.* **63** 2212
- [36] Toleikis S, Bornath T, Döppner T, Düsterer S, Fäustlin R R, Förster E, Fortmann C, Glenzer S H, Göde S, Gregori G, Irsig R, Laarmann T, Lee H J, Li B, Meiwes-Broer K H, Mithen J, Nagler B, Przystawik A, Radcliffe P, Redlin H, Redmer R, Reinholz H, Röpke G, Tavella F, Thiele R, Tiggesbäumker J, Uschmann I, Vinko S M, Witcher T, Zastra U, Ziaja B and Tschentscher T 2010 *J. Phys. B* **43** 194017
- [37] Toennies J P 2013 *Mol. Phys.* **111** 1879--1891
- [38] Kita T, Harada T, Nakano N and Kuroda H 1983 *Appl. Opt.* **22** 512--513
- [39] MacFarlane J J, Golovkin I E and Woodruff P R 2006 *J. Quant. Spectr. Rad. Transf.* **99** 381--397
- [40] MacFarlane J J, Golovkin I E, Wang P, Woodruff P R and Pereyra N A 2007 *High Energ. Dens. Phys.* **3** 181--190
- [41] Wang P 1991 *Computation and application of atomic data for inertial confinement fusion plasmas* Ph.D. thesis University of Wisconsin
- [42] Fischer C F 1978 *Comp. Phys. Comm.* **14** 145--153
- [43] Abdallah Jr J, Clark R E H and Cowan R D 1988 Theoretical atomic physics code development I. cats: Cowan atomic structure code (la--11436-m-vol1)
- [44] Wang P, MacFarlane J J and Moses G A 1992 *Rev. Sci. Instr.* **63** 5059--5061
- [45] Wang P, MacFarlane J J and Moses G A 1993 *Phys. Rev. E* **48** 3934--3942
- [46] Kramida A, Ralchenko Y, Reader J and NIST ASD Team 2017 NIST Atomic Spectra Database (ver. 5.3), [Online]. Available: <http://physics.nist.gov/asd>. National Institute of Standards and Technology, Gaithersburg, MD.
- [47] Köller L, Schumacher M, Köhn J, Teuber S, Tiggesbäumker J and Meiwes-Broer K H 1999 *Phys. Rev. Lett.* **82** 3783--3786
- [48] Griem H R 1997 *Principles of Plasma Spectroscopy* (Cambridge University Press)